Lifetimes of low-lying excited states in $^{86}_{36}Kr_{50}$

J. Henderson,[1,2,*] A. Chester,[3] G. C. Ball,[2] R. Caballero-Folch,[2] T. Domingo,[3] T. E. Drake,[4] L. J. Evitts,[2,5] A. B. Garnsworthy,[2] G. Hackman,[2] S. Hallam,[2,5,†] M. Moukaddam,[2,‡] P. Ruotsalainen,[2,§] J. Smallcombe,[2] J. K. Smith,[2,‖] K. Starosta,[3,¶] C. E. Svensson,[6] and J. Williams[3]

[1]*Lawrence Livermore National Laboratory, Livermore, California 94550, USA*
[2]*TRIUMF, Vancouver, British Columbia, Canada V6T 2A3*
[3]*Department of Chemistry, Simon Fraser University, Burnaby, British Columbia, Canada V5A 1S6*
[4]*Department of Physics, University of Toronto, Toronto, Ontario M5S 1A7, Canada*
[5]*Department of Physics, University of Surrey, Guildford GU2 7XH, United Kingdom*
[6]*Department of Physics, University of Guelph, Guelph, Ontario, Canada N1G 2W1*

(Received 10 January 2018; published 16 April 2018)

Background: The evolution of nuclear magic numbers at extremes of isospin is a topic at the forefront of contemporary nuclear physics. $N = 50$ is a prime example, with increasing experimental data coming to light on potentially doubly magic ^{100}Sn and ^{78}Ni at the proton-rich and proton-deficient extremes, respectively; however, experimental discrepancies exist in the data for less exotic systems.
Purpose: In ^{86}Kr the $B(E2; 2_1^+ \rightarrow 0_1^+)$ value—a key indicator of shell evolution—has been experimentally determined by two different methodologies, with the results deviating by 3σ. Here, we report on a new high-precision measurement of this value, as well as the first measured lifetimes and hence transition strengths for the 2_2^+ and $3_{(2)}^-$ states in the nucleus.
Methods: The Doppler-shift attenuation method was implemented using the TRIUMF-ISAC γ-ray escape-suppressed spectrometer (TIGRESS) γ-ray spectrometer and the TIGRESS integrated plunger device. High-statistics Monte Carlo simulations were utilized to extract lifetimes in accordance with state-of-the-art methodologies.
Results: Lifetimes of $\tau(2_1^+) = 336 \pm 4(\text{stat.}) \pm 20(\text{sys.})$ fs, $\tau(2_2^+) = 263 \pm 9(\text{stat.}) \pm 19(\text{sys.})$ fs, and $\tau(3_{(2)}^-) = 73 \pm 6(\text{stat.}) \pm 32(\text{sys.})$ fs were extracted. This yields a transition strength for the first-excited state of $B(E2; 2_1^+ \rightarrow 0_1^+) = 259 \pm 3(\text{stat.}) \pm 16(\text{sys.})\ e^2\ \text{fm}^4$.
Conclusions: The measured lifetime disagrees with the previous Doppler-shift attenuation method measurement by more than 3σ, while agreeing well with a previous value extracted from Coulomb excitation. The newly extracted $B(E2; 2_1^+ \rightarrow 0_1^+)$ value indicates a more significant reduction in the $N = 50$ isotones approaching $Z = 40$.

DOI: 10.1103/PhysRevC.97.044311

I. INTRODUCTION

Determining the evolution of the nuclear magic numbers far from the line of β stability is the subject of much experimental and theoretical effort. In particular, the advent of the next generation of radioactive ion beam facilities presents the promise of further study of this evolution at the extremes of isospin. So-called "islands of inversion" are now well established at $N = 8$, $N = 20$, and $N = 28$ [1–3], all of which correspond to major shell-closures at the line of stability, as well as the subshell closure at $N = 40$ [4]. The $N = 50$ shell may also be expected to exhibit a similar reduction in the influence of the nominal magic numbers (see, e.g., Refs. [5,6]), incorporating the neutron-deficient (nominally) doubly magic ^{100}Sn and the neutron-rich ^{78}Ni. Key experimental observables in the mapping of nuclear shell evolution include excited 2_1^+ state energies and $E2$ transition strengths [e.g., $B(E2; 2^+ \rightarrow 0^+)$]. While experimental $B(E2)$ data are lacking for ^{78}Ni, other experimental observables as well as theoretical calculations point towards the nucleus behaving as doubly magic, albeit with the potential for shape coexistence [6–9]. To properly assess the evolution of nuclear shell closures the experimental determination of these observables at stability where "normal" configurations dominate is thus important.

The evolution of $B(E2)$ values in magic nuclei can be described by the seniority scheme. In this regime, where excitations are described purely in terms of the breaking of coupled pairs of antialigned nucleons, $B(E2; 2_1^+ \rightarrow 0_1^+)$

*henderson64@llnl.gov
†Present address: Department of Physics, University of Surrey, Guildford, GU2 7XH, United Kingdom.
‡Present address: Department of Physics, University of Surrey, Guildford, GU2 7XH, United Kingdom.
§Present address: Department of Physics, University of Jyväskylä, FIN-40014 Finland.
‖Present address: Physics Department, Reed College, Portland OR, 97202, USA.
¶starosta@sfu.ca

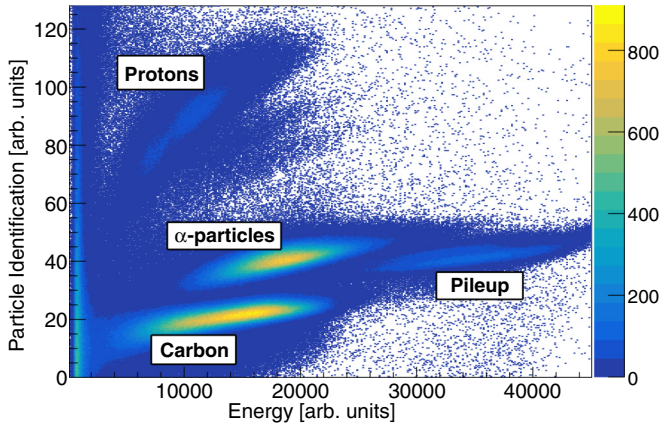

FIG. 1. The particle identification (PID) parameter determined from wave-form fitting plotted against the energy in the CsI(Tl) detectors with the major loci indicated.

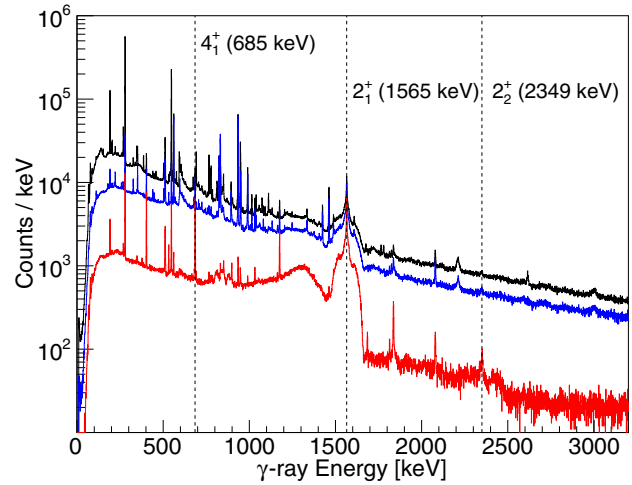

FIG. 2. Black: Add-back γ-ray spectrum. Blue: Requiring a good time coincidence with a CsI(Tl) event and an RF beam bucket. Red: Requiring the coincident CsI(Tl) event that has a PID parameter consistent with the carbon detection. The γ-ray peaks arising from the decays of states of interest are indicated. Note that γ rays originating from the 3^- state are not resolvable from those from the 2_1^+ state in this figure.

transitions are expected to follow a systematic parabolic trend, with a maximum at the midshell. This is exemplified in the tin isotopes, where the parabolic behavior is clearly apparent [10]. A similar behavior would be expected of the $N = 50$ isotones, where one might expect a parabolic maximum to occur at around $Z = 38$ and $Z = 40$. In reality, this picture is complicated by the strength of the $Z = 40$ subshell closure, which causes ^{90}Zr to exhibit many of the properties expected of a doubly magic nucleus. Thus, rather than a maximum, the $B(E2; 2_1^+ \rightarrow 0_1^+)$ value for ^{90}Zr is the lowest yet observed in the $N = 50$ isotonic chain. While the $B(E2)$ for ^{90}Zr is a local minimum, it is approximately a factor of 4 larger than that predicted in ^{78}Ni [6]. The behavior of the $N = 50$ isotones about $Z = 40$ might then be described in analogy to the generalized seniority description of a potential "dip" around $A = 116$ in the tin isotopes (see, e.g., Ref. [11]), with the reduced depth of the $B(E2)$ minimum at $Z = 40$ explained by particle-hole excitations violating the seniority scheme in a manner similar to that discussed in Ref. [12].

The depth of the minimum at $Z = 40$ relates to the $B(E2; 2_1^+ \rightarrow 0_1^+)$ values of the $N = 50$, $30 \leqslant Z \leqslant 38$ and $N = 50$, $42 \leqslant Z \leqslant 48$ isotones as well as ^{90}Zr. Of the even-even $N = 50$ isotones, $B(E2; 2_1^+ \rightarrow 0_1^+)$ data are available for seven nuclides, from ^{80}Zn through to ^{92}Mo. In the region between $Z = 32$ and $Z = 38$, $B(E2)$ values are relatively constant as is expected from the seniority scheme. Data for heavier isotones are limited to ^{92}Mo, preventing any systematic comparison. The data for $^{86}_{36}$Kr and $^{88}_{38}$Sr are found to be inconsistent, with $B(E2)$ values determined from a lifetime measurement using the Doppler-shift attenuation method (DSAM) technique [13–15] found to deviate from that determined using Coulomb excitation [16,17] at a 3σ level in ^{86}Kr and at a 1σ level in ^{88}Sr and with the Coulomb-excitation-derived $B(E2)$ values being larger in both cases. A figure showing $N = 50$, $B(E2; 2_1^+ \rightarrow 0_1^+)$ systematics is shown in the discussion section of this paper.

In the present work, we therefore undertook to remeasure the lifetime of the 2_1^+ state in ^{86}Kr using the DSAM technique, following population by unsafe Coulomb excitation. The major benefit of this population mechanism is that Coulomb-excitation cross sections reduce as one requires more excitation energy or further steps of excitation, greatly reducing the impact of feeding from higher-lying states on the lifetimes measured for the states of interest. A benefit for the present measurement over that of Ref. [13] is the use of a 4π high-purity germanium (HPGe) array, greatly enhancing sensitivity to near-degenerate states that might only be resolved at either forward or backward angles. The analysis of this work is very similar to that described in Ref. [18] but utilizes the DSAM technique rather than the recoil-distance method.

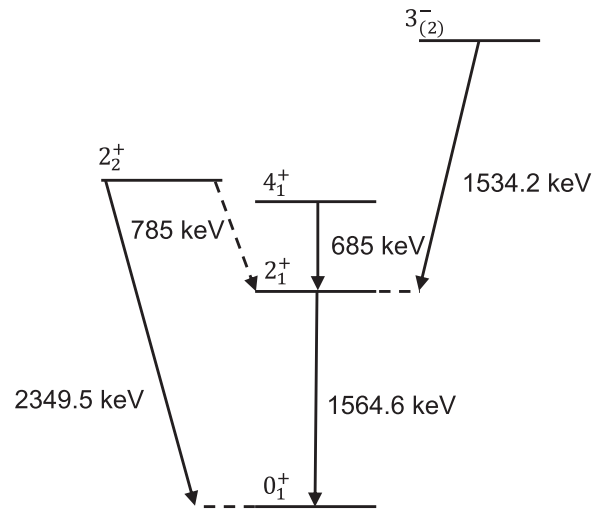

FIG. 3. Reduced level scheme indicating the states of interest in the present work. Dashed transitions indicate γ rays that were not observed but for which feeding contributions were incorporated into the line-shape analysis.

II. EXPERIMENTAL DETAILS

States of interest were populated through the unsafe Coulomb excitation of ^{86}Kr in inverse kinematics. A beam of ^{86}Kr ions was produced by the TRIUMF offline ion source [19], accelerated to 256.7 MeV by the TRIUMF-ISAC accelerator chain and delivered to the TRIUMF-ISAC γ-ray escape-suppressed spectrometer (TIGRESS) facility [20]. For the present measurement, TIGRESS contained 11 32-fold segmented HPGe clover detectors, with 3 located at 45°, 5 at 90°, and 3 at 135° relative to the beam axis. TIGRESS surrounded the TIGRESS integrated plunger (TIP) [21] setup, which consisted of a wall of 24 16 × 14 mm^2, 2-mm-thick CsI(Tl) detectors located 51.7 mm downstream of the target. The beam was impinged onto a 2.165-μm (0.5-mg/cm^2)-thick amorphous carbon target, backed by a 14.917-μm (28.8-mg/cm^2)-thick gold foil to stop the beamlike particles [22]. A beam intensity of approximately 100 ppA was maintained for 30 h. Data were acquired using the TIGRESS digital data acquisition system [23] with a particle-γ coincidence condition required. Detector wave forms were collected for both the HPGe and CsI(Tl) detectors, as well as coincident accelerator-RF wave forms. A similar experimental configuration using the TIP, TIGRESS, and the same target used in the present work is discussed in Ref. [24].

III. ANALYSIS

Data were unpacked and analyzed using the in-house GRSISORT analysis software [25], built on the ROOT framework [26]. Events were constructed on the basis of a trigger identifier, provided by the TIGRESS acquisition system. Precise relative timing information was extracted through the fitting of the CsI(Tl), HPGe, and RF wave forms. Particle-γ pairs were constructed on the basis of this timing information, which were themselves coincident with an RF pulse and, thus, a beam bucket from the accelerator chain. Wave-form fitting also allowed for particle identification (PID) on the basis of the well-understood response of CsI(Tl) (see, e.g., Ref. [21]). A PID plot for the innermost four CsI(Tl) detectors is shown in Fig. 1.

To maximize peak-to-background, HPGe signals were added back on the basis of both the time of the detection event and the subclover position provided by the segmented detector anodes. The added-back data were then time gated on the basis of both an RF beam bucket and a time-coincident CsI(Tl) detector hit. Finally, a PID gate was applied, requiring the coincident CsI(Tl) event to be consistent with a carbon recoil. The γ-ray gating process is shown in Fig. 2. The consequence of this series of filters was a very clean γ-ray spectrum. Some time-random β-decay lines remain in the spectrum; however these do not interfere with the DSAM line-shape analysis. The only discernible background arising from in-flight decays (i.e., not the result of time-random β decays) were weak γ-ray lines consistent with a single-proton transfer reaction into ^{87}Rb, the isotonic neighbor of ^{86}Kr. Where resolvable these weak lines were fitted with a simple Gaussian and included in the fitting of the Monte Carlo simulations. No strong background lines were observed to interfere with the decays that will be discussed.

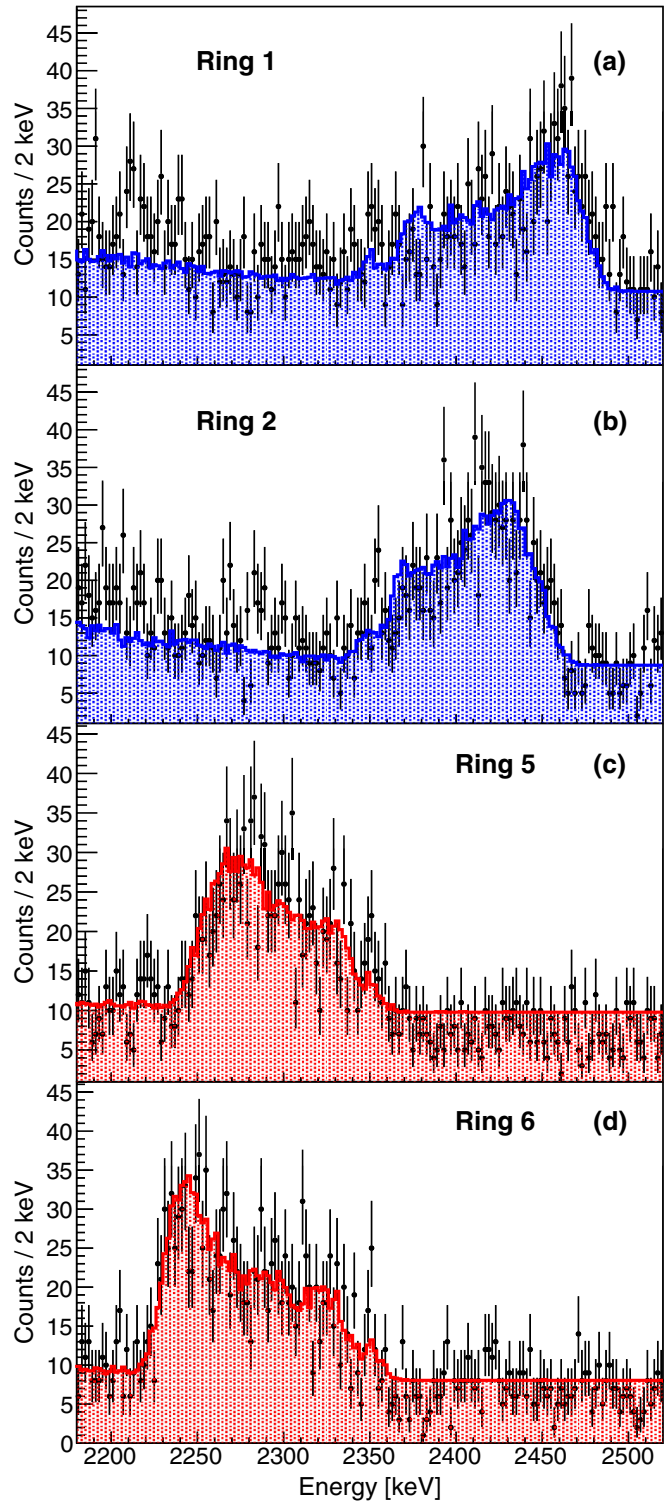

FIG. 4. Simulated line shape (filled) plotted along with the experimental data (data points) for rings 1, 2, 5, and 6 [panels (a)–(d), respectively] for a simulated lifetime, $\tau(2_2^+) = 260$ fs.

Observed in the data were four transitions from the decay of excited states of ^{86}Kr: $2_1^+ \rightarrow 0_1^+$ ($E_\gamma = 1564.67$ keV), $4_1^+ \rightarrow 2_1^+$ ($E_\gamma = 685.35$ keV), $2_2^+ \rightarrow 0_1^+$ ($E_\gamma = 2349.47$ keV), and $3_{(2)}^- \rightarrow 2_1^+$ ($E_\gamma = 1534.24$ keV). Of these transitions, only the

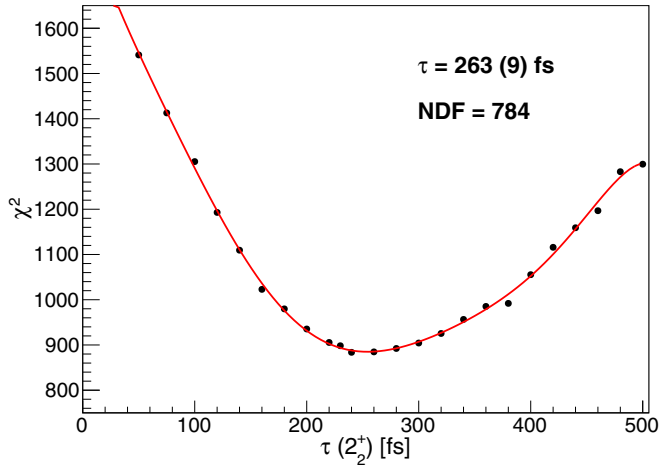

FIG. 5. χ^2 plotted against the simulated lifetime of the 2_2^+ state for all four sensitive rings (see Fig. 4). As indicated, the χ^2 minimum is found to correspond to $\tau = 263(9)$ fs. Once systematic uncertainties are incorporated the final value becomes $\tau = 263(9)\ (19)$ fs.

$4_1^+ \rightarrow 2_1^+$ transition had no in-flight line-shape component, consistent with its previously determined half-life of 3.1 ns. The remaining three transitions were thus suitable for a DSAM analysis. A reduced level scheme showing the states observed in the present work is given in Fig. 3.

The techniques used to analyze the DSAM spectra are outlined in detail in Refs. [18,27]. High-statistics GEANT4 simulations were performed using a detailed model of the TIGRESS and TIP spectrometers. For the purposes of the DSAM analysis, only the inner eight TIP CsI(Tl) detectors were used—for the remaining detectors the particle-identification plot (see Fig. 1) did not give good separation for the carbon nuclei, and losses due to thresholds could not be consistently accounted for. The simulated GEANT4 spectra were smeared according to the observed HPGe detector resolution prior to comparisons with the experimental data. For comparison with simulations, TIGRESS was separated into six rings corresponding to the downstream- and upstream-most rings of the 45°, 90°, and

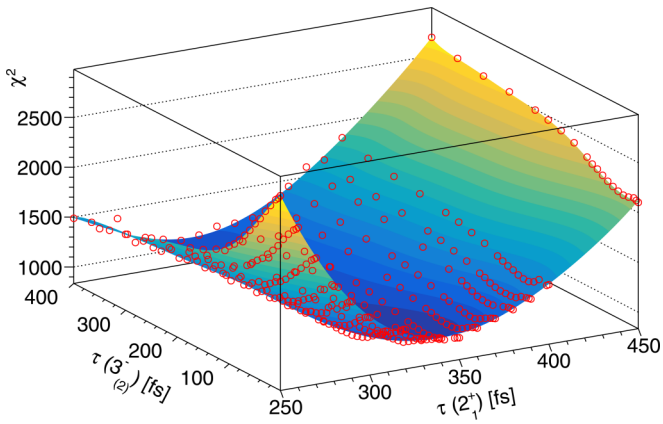

FIG. 6. The χ^2 surface fitted to the minimized χ^2 values (red circles) used to determine the lifetime minima for the overlapping 2_1^+ and $3_{(2)}^-$ line shapes.

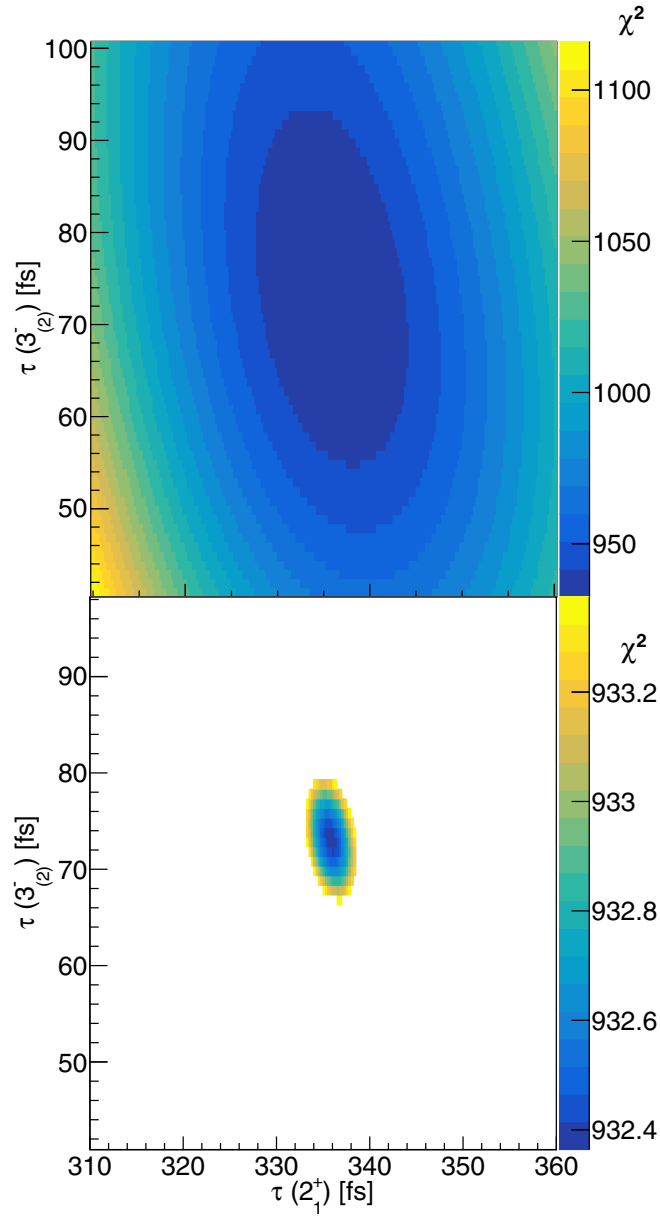

FIG. 7. Top: The χ^2 surface as determined from the fit shown in Fig. 6 in the region of $\chi^2_{\rm min}$. Bottom: The $\chi^2 \leqslant \chi^2_{\rm min} + 1$ region from which the minimum and associated statistical uncertainties were determined.

135° clovers, with ring 1 being the most downstream and ring 6 the most upstream. No sensitivity to lifetimes was found for the rings about 90°. Angular correlation effects were not found to be important and were not included in the further analysis.

A. The $2_2^+ \rightarrow 0_1^+$ transition

The $2_2^+ \rightarrow 0_1^+$ ($E_\gamma = 2349$ keV) transition was well separated from the other lines and could thus be analyzed independently. No feeding transition to the 2_1^+ state was observed ($E_\gamma = 749$ keV); however, this would not be expected to be visible above background. Simulated spectra were constructed from 5×10^6 CsI(Tl)-HPGe coincidences. The spectra were then fit to the experimental data for all four sensitive rings (1,

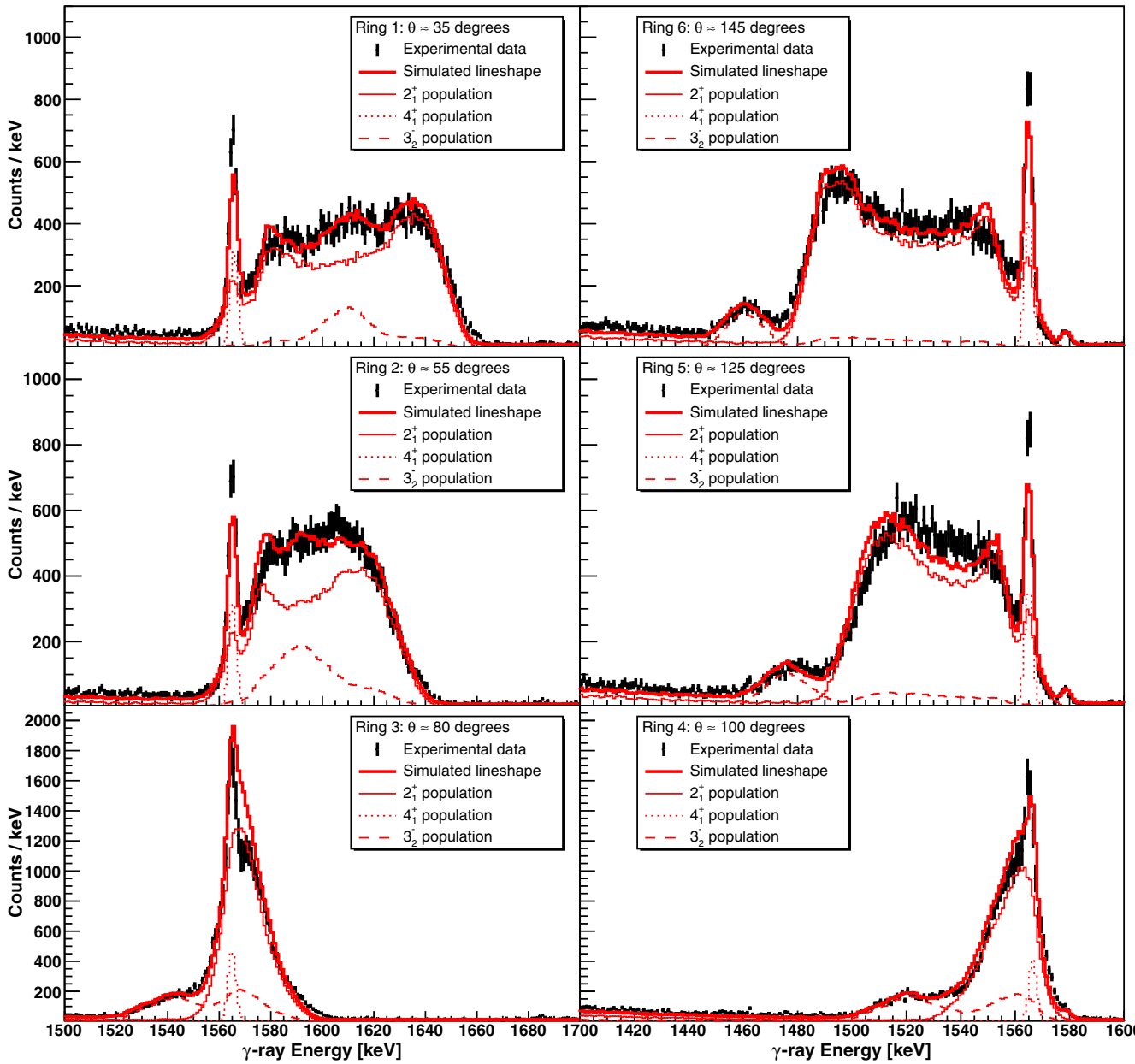

FIG. 8. Fitted line shape (thick solid, red line) corresponding to the minimized χ^2 overlayed on the experimental data (black points) for the six rings in TIGRESS. Also shown are the primary contributions to the line shape arising from direct population of the 2_1^+ state (thin solid, red line), population via the 4_1^+ state (dotted, red line) and via the $3_{(2)}^-$ state (dashed, red line). Details of the parameters varied in the fits are provided in the text. Rings 3 and 4 were insensitive to the state lifetimes and were not included in the χ^2 surface shown in Fig. 6.

2, 5, and 6) simultaneously. The parameters in the fits were a scaling parameter, a zeroth-order polynomial background that was constrained (but not fixed) prior to the fit, and an E_γ-shift parameter to account for any low-level mismatch between the simulated and experimental energies—in particular to allow for binning effects. Due to the low level of statistics for this transition, the use of a maximum-likelihood method was essential, as described in Ref. [18]. The simulated line shape corresponding to the maximized log-likelihood is shown in Fig. 4. To account for the fact that the reduced $\chi^2_{\rm min}/\nu = 1.12 > 1$, the statistical uncertainties were inflated by a factor of $\sqrt{\chi^2_{\rm min}/\nu} = 1.06$ following the prescription of Ref. [28], yielding a final lifetime of 263 fs with $\delta\tau_{\rm stat} = 9$ fs (see Fig. 5).

B. The $2_1^+ \rightarrow 0_1^+$ and $3_{(2)}^- \rightarrow 2_1^+$ transitions

The $2_1^+ \rightarrow 0_1^+$ (1564 keV) and $3_{(2)}^- \rightarrow 2_1^+$ (1534 keV) transitions lie too close in energy for their respective line shapes to be fully disentangled. Indeed, in the downstream (rings 1 and 2) data, the $3_{(2)}^- \rightarrow 2_1^+$ transition could not be visually identified. Consequently, and because the $3_{(2)}^- \rightarrow 2_1^+$ transition feeds the 2_1^+ state, the two transitions had to be analyzed simultaneously. No indication for any competing branch in the decay of the $3_{(2)}^-$

state was observed, nor is there any indication of such a decay in the literature. The branch was therefore assumed to be 100% in the present work. This is consistent with the literature $B(E3; 3^- \rightarrow 0^+)$ value extracted from proton scattering [29–31] that yields a partial $E3$ lifetime of approximately 120 ps and a ground-state branch of less than 0.1%.

Because the two line-shapes overlapped it was necessary for all rings to be analyzed simultaneously, with the backward rings being particularly sensitive to short $3^-_{(2)}$ lifetimes and the forward rings placing limits on long lifetimes. Simulated spectra were again generated with 5×10^6 CsI(Tl)-γ coincident events, with the feeding and subsequent decay of the 2^+_1 state included in the simulation of the 3^- decay (see Ref. [27]). Three hundred forty simulated data sets were therefore created for the 3^- decay, corresponding to 17 potential 2^+_1 lifetimes and 20 potential $3^-_{(2)}$ lifetimes, with a further 17 simulated datasets corresponding to direct population of the 2^+_1 state. Feeding of the 2^+_1 state from the stopped ($t_{1/2} = 3.1$ ns) 4^+_1 state was also simulated. Feeding from the 2^+_2 state was included but was found to have very little effect on the final result.

The simulated data were then fit to the experimental spectra, with all four rings fitted simultaneously. For each ring, the following parameters were independently varied to achieve the best fit: a scaling parameter for the 2^+_1 direct feeding, a scaling parameter for the $3^+_{(2)}$ decay (including the resultant decay of the 2^+_1 state), a zeroth-order polynomial background, and an E_γ-shift parameter to allow for low-level mismatch between simulated and experimental energies. The 4^+ feeding contribution was fixed for all rings based on a fit to the intensity of the $4^+_1 \rightarrow 2^+_1$ decay line.

A χ^2 surface was fit to the resultant χ^2 values, as shown in Fig. 6. From this, the $\chi^2_{\min} \leqslant \chi^2 \leqslant \chi^2_{\min} + 1$ range could then be extracted to determine the resultant state lifetimes and their associated uncertainties. Figure 7 shows the total and 1σ surface in the vicinity of the minimum with the fitted line shapes shown in Fig. 8, along with the major contributions to the fit. The resultant lifetimes are $\tau(2^+_1) = 336 \pm 3$ fs and $\tau(3^-_{(2)}) = 73 \pm 5$ fs. To account for the fact that the reduced $\chi^2_{\min}/\nu = 1.6 > 1$, the statistical uncertainties were inflated by a factor of $\sqrt{\chi^2_{\min}/\nu} = 1.3$ following the prescription of Ref. [28], yielding final lifetimes of $\tau(2^+_1) = 336$ fs with $\delta\tau_{\text{stat}}(2^+_1) = 4$ fs and $\tau(3^-_{(2)}) = 73$ fs with $\delta\tau_{\text{stat}}(3^-_{(2)}) = 6$ fs.

C. Systematic uncertainties

Uncertainties on the present measurement are dominated by systematic effects. The primary systematic uncertainties in the present measurement arise from uncertainties in the stopping powers for krypton in amorphous carbon and gold. The fast (large v/c) component to the line shapes was found to be sensitive to the stopping in carbon and was varied during the simulation procedure. All results thus far correspond to a stopping power of 60% of that included by default within the GEANT4 libraries that was found to best reproduce the data. Full simulations were performed for 40%, 50%, 60%, 70%, and 80% of the nominal carbon stopping powers in GEANT4. Based on simulations performed with these stopping powers systematic uncertainties of $\delta\tau(2^+_1) = 7$ fs and $\delta\tau(3^-_{(2)}) = 4$ fs were estimated. A similar analysis was performed for the lifetime of the 2^+_2 state, yielding an uncertainty from the carbon stopping powers of $\delta\tau(2^+_2) = 5$ fs. No clear sensitivity was discernible in the fitting to the stopping of krypton in gold. We attribute a 5% additional systematic uncertainty to the final results from potential discrepancies in gold stopping powers. A small systematic uncertainty (2 fs) is also associated with the choice of polynomial used to fit the χ^2 surface in Fig. 6. We find a small sensitivity to feeding from the 2^+_2 state, from which we attribute a 1-fs systematic uncertainty to the 2^+_1 and 3^- lifetimes. Finally, it is found that for the $3^-_{(2)}$ state there is a discrepancy between the lifetime extracted using rings 1 and 6 [35° and 145°, 96(10) fs] and that extracted using rings 2 and

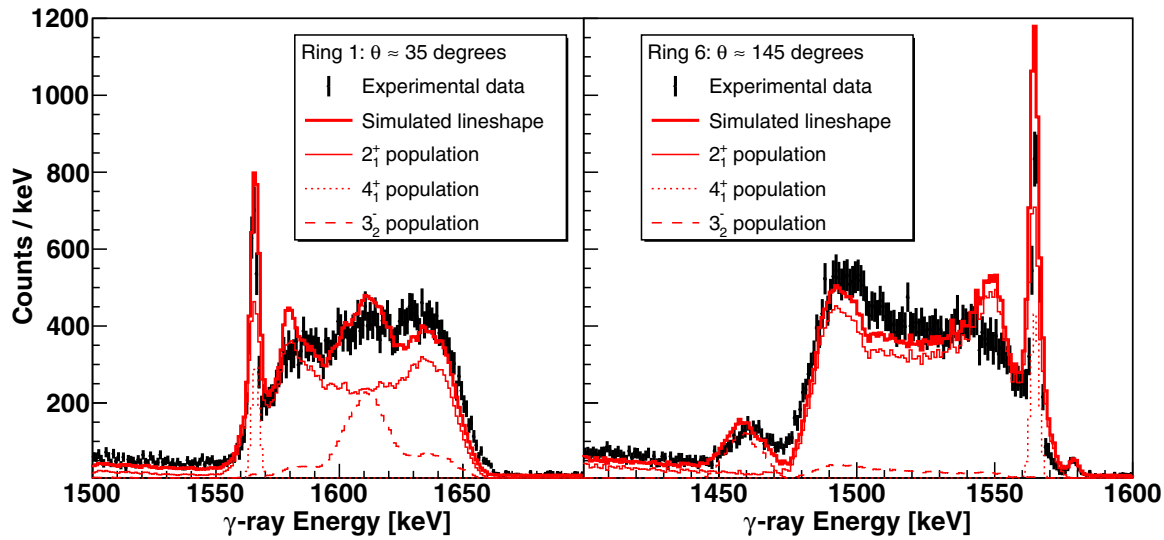

FIG. 9. Line shapes for a 2^+_1 state lifetime of 450 fs [Ref. [13]: $\tau(2^+_1) = 440(25)$ fs] for the downstream- and upstream-most rings. A $3^-_{(2)}$ state lifetime of $\tau(3^-_{(2)}) = 10$ fs is used, corresponding to the approximate χ^2 minimum in Fig. 6 at $\tau(2^+_1) = 450$ fs. The poorer quality of the fit for both the 2^+_1 and 3^- components is clear in comparison to that of Fig. 8.

TABLE I. Lifetimes and reduced transition probabilities as determined in the present work compared to literature values, where available. The branching and mixing ratios for the decay of the 2_2^+ state were taken from Ref. [32]. The quoted $B(E1)$ for the $3^- \rightarrow 2^+$ transition assumes a pure $E1$. No other decay branches for the $3^-_{(2)}$ state are known, nor were any observed in the present work. Here, the first quoted uncertainty corresponds to statistics and the second quoted uncertainty corresponds to systematics. Uncertainties due to branching and mixing ratios are incorporated into the systematic uncertainties.

Transition	τ (fs)		$B(E2)$ (e^2 fm^4)		Ref.
	This work	Lit.	This work	Lit.	
$2_1^+ \rightarrow 0_1^+$	336 (4)(20)	444 (25)	259 (3)(16)	196(11)	[13]
		341 (27)		256(20)	[16]
		396 (108)		220(60)	[33]
$2_2^+ \rightarrow 0_1^+$	263 (9)(19)		27(1)(3)		
$2_2^+ \rightarrow 2_1^+$	263 (9)(19)		38(1)(27)		
Transition	τ (fs)		$B(E1)$ (e^2 fm^2)		
$3^-_{(2)} \rightarrow 2_1^+$	73 (6)(32)		0.0024(2)(11)		
Transition	τ (fs)		$B(M1)$ (μ_N^2)		
$2_2^+ \rightarrow 2_1^+$	263 (9)(19)		0.17 (1)(13)		

5e [55° and 125°, 53(11) fs]. We attribute a 20-fs systematic uncertainty, accordingly. The equivalent discrepancy for the 2_1^+ and 2_2^+ states is found to be approximately 2 fs. We therefore quote final systematic uncertainties of $\delta\tau_{(\text{sys.})}(2_1^+) = 20$ fs, $\delta\tau_{(\text{sys.})}(2_2^+) = 19$ fs, and $\delta\tau_{(\text{sys.})}(3^-_{(2)}) = 32$ fs, giving results of $336 \pm 4(\text{stat.}) \pm 20(\text{sys.})$ fs for the 2_1^+ state, $263 \pm 9(\text{stat.}) \pm 19(\text{sys.})$ fs for the 2_2^+ state, and $73 \pm 6(\text{stat.}) \pm 32(\text{sys.})$ fs for the 3_2^- state (see Table I).

IV. DISCUSSION

The present results deviate from those determined in Ref. [13] by more than 3 standard deviations. We note, however, that the measurement reported in Ref. [13] was unable to resolve the 3^- state observed in the present work. The failure to include this contribution in the lifetime determination of the present work—even at relatively low levels—would result in the extraction of a longer lifetime from the analysis. This highlights the importance of using HPGe arrays with detectors at both forward and backward angles in DSAM analyses. To demonstrate to the reader the incompatibility of the lifetime quoted in Ref. [13] with the present data, Fig. 9 shows simulated line shapes corresponding to a lifetime of 450 fs. The lifetime extracted in the present work is in good agreement with both the Coulomb-excitation works of Refs. [16,33]. Excluding the DSAM result of Ref. [13] for the above-stated reasons, we determine a new weighted average lifetime, $\tau_{2_1^+} = 339 \pm 16$ fs.

Figure 10 shows $B(E2; 2_1^+ \rightarrow 0_1^+)$ values for the $N = 50$ isotones, where known. Clearly, the present result and its associated conclusions represents a significant deviation from the accepted values, with ^{86}Kr now having among the larger $B(E2)$ values of the $N = 50$ nuclides. Also shown is a predicted $B(E2; 2_1^+ \rightarrow 0_1^+)$ value for ^{78}Ni [6]. Clearly, the $Z = 40$ minimum is not as pronounced as that expected for

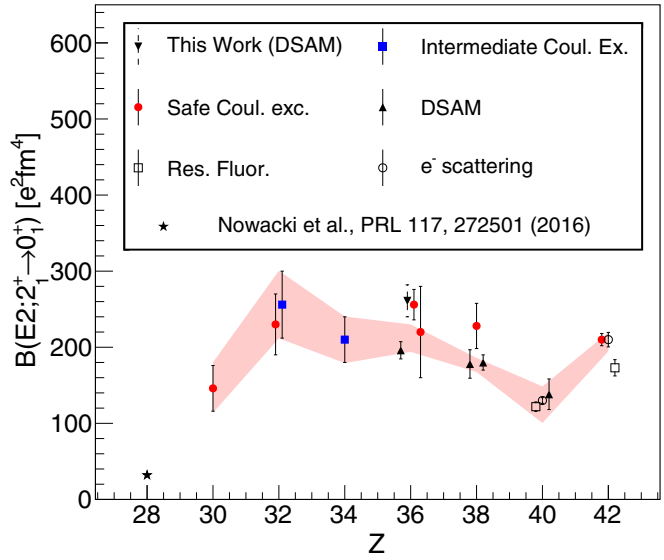

FIG. 10. $B(E2; 2_1^+ \rightarrow 0_1^+)$ value systematics for the $N = 50$ isotones. The uncertainties on the present result are dominated by systematics (dashed lines) but agree well with previous Coulomb-excitation data. The evaluated data range is indicated by the shaded band. Experimental data were taken from Refs. [13–17,33–43]. Also shown is the $B(E2; 2_1^+ \rightarrow 0_1^+)$ value predicted for ^{78}Ni in Ref. [6].

$Z = 28$, but the present $B(E2)$ measurement indicates a more significant minimum relative to the midshell nuclei. In light of the present result, a remeasurement of the $B(E2; 2_1^+ \rightarrow 0_1^+)$ values in ^{88}Sr and ^{84}Se would be of interest to confirm behavior approaching $Z = 40$ and in the midshell region, respectively.

V. CONCLUSIONS

We have remeasured the lifetime of the first-excited state in ^{86}Kr using the DSAM following population in unsafe Coulomb excitation. Our result agrees with previous Coulomb-excitation measurements and disagrees with a previous DSAM measurement at the 3σ level. We hypothesize that this discrepancy may arise from the failure of the previous measurement to resolve a feeding state with a line shape that overlaps with the state of interest. We were further able to extract lifetimes for the $3^-_{(2)}$ and 2_2^+ states and determine transition strengths accordingly. Our new data indicate a more precipitous reduction in $B(E2)$ strength in the $N = 50$ isotones approaching the $Z = 40$ subshell closure than was previously thought to occur, resulting in a more pronounced minimum at ^{90}Zr. This new lifetime may also affect the conclusions of g-factor measurements that need to account for the lifetimes of the states of interest (e.g., Refs. [13,37]) in the transient-field technique.

ACKNOWLEDGMENTS

The authors thank the TRIUMF beam delivery group for their efforts in providing high-quality beams. This work has been supported by the Natural Sciences and Engineering Research Council of Canada (NSERC), The Canada Foundation for Innovation, and the British Columbia Knowledge

Development Fund. TRIUMF receives federal funding via a contribution agreement through the National Research Council of Canada. The work at LLNL is under Contract No. DE-AC52-07NA27344.

[1] A. Navin *et al.*, Phys. Rev. Lett. **85**, 266 (2000).
[2] C. Thibault *et al.*, Phys. Rev. C **12**, 644 (1975).
[3] B. Bastin *et al.*, Phys. Rev. Lett. **99**, 022503 (2007).
[4] S. Naimi, G. Audi, D. Beck, K. Blaum, C. Böhm, C. Borgmann, M. Breitenfeldt, S. George, F. Herfurth, A. Herlert, A. Kellerbauer, M. Kowalska, D. Lunney, E. Minaya Ramirez, D. Neidherr, M. Rosenbusch, L. Schweikhard, R. N. Wolf, and K. Zuber, Phys. Rev. C **86**, 014325 (2012).
[5] C. Santamaria *et al.*, Phys. Rev. Lett. **115**, 192501 (2015).
[6] F. Nowacki, A. Poves, E. Caurier, and B. Bounthong, Phys. Rev. Lett. **117**, 272501 (2016).
[7] G. Hagen, G. R. Jansen, and T. Papenbrock, Phys. Rev. Lett. **117**, 172501 (2016).
[8] A. Welker, N. A. S. Althubiti, D. Atanasov, K. Blaum, T. E. Cocolios, F. Herfurth, S. Kreim, D. Lunney, V. Manea, M. Mougeot, D. Neidherr, F. Nowacki, A. Poves, M. Rosenbusch, L. Schweikhard, F. Wienholtz, R. N. Wolf, and K. Zuber, Phys. Rev. Lett. **119**, 192502 (2017).
[9] L. Olivier *et al.*, Phys. Rev. Lett. **119**, 192501 (2017).
[10] R. Kumar, M. Saxena, P. Doornenbal, A. Jhingan, A. Banerjee, R. K. Bhowmik, S. Dutt, R. Garg, C. Joshi, V. Mishra, P. J. Napiorkowski, S. Prajapati, P. A. Soderstrom, N. Kumar, and H. J. Wollersheim, Phys. Rev. C **96**, 054318 (2017).
[11] I. O. Morales, P. Van Isacker, and I. Talmi, Phys. Lett. B **703**, 606 (2011).
[12] H. Mach *et al.*, Phys. Rev. C **95**, 014313 (2017).
[13] T. J. Mertzimekis, N. Benczer-Koller, J. Holden, G. Jakob, G. Kumbartzki, K.-H. Speidel, R. Ernst, A. Macchiavelli, M. McMahan, L. Phair, P. Maier-Komor, A. Pakou, S. Vincent, and W. Korten, Phys. Rev. C **64**, 024314 (2001).
[14] A. I. Kucharska, J. Billowes, and M. A. Grace, J. Phys. G **14**, 65 (1988).
[15] G. J. Kumbartzki, K.-H. Speidel, N. Benczer-Koller, D. A. Torres, Y. Y. Sharon, L. Zamick, S. J. Q. Robinson, P. Maier-Komor, T. Ahn, V. Anagnostatou, C. Bernards, M. Elvers, P. Goddard, A. Heinz, G. Ilie, D. Radeck, D. Savran, V. Werner, and E. Williams, Phys. Rev. C **85**, 044322 (2012).
[16] J. Cheng-lie and S. Pontoppidan, Phys. Rev. C **24**, 1350 (1981).
[17] P. R. Christensen *et al.*, Nucl. Phys. A **207**, 433 (1973).
[18] A. Chester *et al.*, Nucl. Instrum. Methods Phys. Res., Sect. A **882**, 69 (2018).
[19] K. Jayamanna *et al.*, Rev. Sci. Instrum. **79**, 02C711 (2008).
[20] G. Hackman and C. E. Svensson, Hyperfine Interact. **225**, 241 (2014).
[21] P. Voss *et al.*, Nucl. Instrum. Methods Phys. Res., Sect. A **746**, 87 (2014).
[22] J. Greene, P. Voss, and K. Starosta, J. Radiol. Nucl. Chem. **299**, 1121 (2014).
[23] J. P. Martin, C. Mercier, N. Starinski, C. J. Pearson, and P. A. Amaudruz, IEEE Trans. Nucl. Sci. **55**, 84 (2008).
[24] P. Voss *et al.*, Phys. Rev. C **96**, 024305 (2017).
[25] GRSISort, https://github.com/GRIFFINCollaboration/GRSISort/.
[26] R. Brun and F. Rademakers, Nucl. Instrum. Methods Phys. Res., Sect. A **389**, 81 (1997).
[27] J. Williams *et al.*, Nucl. Instrum. Methods Phys. Res., Sect. A **859**, 8 (2017).
[28] C. Patrignani *et al.* (Particle Data Group), Chin. Phys. C **40**, 100001 (2016).
[29] T. Kibédi and R. H. Spear, At. Data Nucl. Data Tables **80**, 35 (2002).
[30] B. K. Arora *et al.*, Phys. Rev. C **10**, 2301 (1974).
[31] S. Matsuki *et al.*, Phys. Lett. B **72**, 319 (1978).
[32] W. Urban, K. Sieja, T. Materna, M. Czerwinski, T. Rzaca-Urban, A. Blanc, M. Jentschel, P. Mutti, U. Köster, T. Soldner, G. de France, G. S. Simpson, C. A. Ur, C. Bernards, C. Fransen, J. Jolie, J.-M. Regis, T. Thomas, and N. Warr, Phys. Rev. C **94**, 044328 (2016).
[33] C. M. Cartwright, P. D. Forsyth, I. Hall, A. D. Irving, and D. G. E. Martin, J. Phys. G **7**, 65 (1981).
[34] A. Gade, T. Baugher, D. Bazin, B. A. Brown, C. M. Campbell, T. Glasmacher, G. F. Grinyer, M. Honma, S. McDaniel, R. Meharchand, T. Otsuka, A. Ratkiewicz, J. A. Tostevin, K. A. Walsh, and D. Weisshaar, Phys. Rev. C **81**, 064326 (2010).
[35] J. van der Walle *et al.*, Phys. Rev. Lett. **99**, 142501 (2007).
[36] E. Padilla-Rodal *et al.*, Phys. Rev. Lett. **94**, 122501 (2005).
[37] G. J. Kumbartzki, N. Benczer-Koller, S. Burcher, A. Ratkiewicz, S. L. Rice, Y. Y. Sharon, L. Zamick, K.-H. Speidel, D. A. Torres, K. Sieja, M. McCleskey, A. Cudd, M. Henry, A. Saastamoinen, M. Slater, A. Spiridon, S. Yu. Torilov, V. I. Zherebchevsky, G. Gürdal, S. J. Q. Robinson, S. D. Pain, and J. T. Burke, Phys. Rev. C **89**, 064305 (2014).
[38] J. Heisenberg, J. Dawson, T. Milliman, O. Schwentker, J. Lichtenstadt, C. N. Papanicolas, J. Wise, J. S. McCarthy, N. Hintz, and H. P. Blok, Phys. Rev. C **29**, 97 (1984).
[39] F. R. Metzger, Nucl. Phys. A **182**, 213 (1972).
[40] G. P. S. Sahota *et al.*, J. Phys. Soc. Jpn. **62**, 2958 (1993).
[41] S. Raman *et al.*, At. Data Nucl. Data Tables **36**, 1 (1987).
[42] F. R. Metzger, Phys. Rev. C **15**, 193 (1977).
[43] T. E. Milliman, Ph.D. thesis, University of New Hampshire, 1987.